

# Structural Stability of V-Amylose Helices in Water-DMSO Mixtures Analyzed by Molecular Dynamics

Markus Tusch, Jens Krüger, and Gregor Fels\*

Department of Chemistry, Faculty of Science, University of Paderborn, Warburger Strasse 100, D-33098 Paderborn, Germany

**ABSTRACT:** Computational techniques have been employed to fundamentally understand the behavior of helically structured amylose in water/DMSO mixtures. Using a computationally generated amylose helix of 55 glucose residues, we have investigated the time-dependent behavior of intra- and intermolecular hydrogen bonds, particularly between O2 and O3 of adjacent glucose molecules and between O6 and neighboring O2 and O3 groups. The helix character was defined by the total number of residually existing hydrogen bonds. Our results parallel the experimental finding that increasing the percentage of DMSO results in increasing helical stability. It can be shown that O6–O2/O3 hydrogen bonds are preferentially lost when the helix starts to unfold to a finally resulting random coil structure. While water is small enough to interact with every hydroxyl group at the helix surface and finally penetrate the helix coil, DMSO can initially only form single hydrogen bonds to part of the OH groups of the amylose molecule, thereby allowing a longer conservation of intramolecular hydrogen bonds that are necessary to maintain the helix. However, given a long enough time for interaction, the helical structure of amylose is lost in water as well as in DMSO, yielding a random orientation of the glucose strand.

## ■ INTRODUCTION

Amylose, naturally occurring as the unbranched component of starch, is a linear polysaccharide consisting of  $\alpha$ -(1 $\rightarrow$ 4)-linked glucose units. Featuring a large number of rotatable glycosidic linkages, the polymer can adopt a virtually unlimited variety of possible conformations. As the actual secondary structure greatly influences the properties of a molecule, the elucidation of amylose conformations has been an objective of extensive research. Most of the available structural information has been obtained with X-ray<sup>1–3</sup> and electron diffraction,<sup>4</sup> which are restricted to the study of crystalline phases. The conformation of amylose in solution, however, still remains uncertain to some extent, as it lacks methods for direct unambiguous determination. Results from static and dynamic light scattering as well as studies of viscosity, sedimentation equilibrium, osmotic pressure, and specific optical rotation led to differing conclusions for amylose in water, ranging from a random coil without any helical character<sup>5</sup> to a random coil built up by helical segments<sup>6</sup> of more than 100 glucose units each.<sup>7</sup> The latter conclusion has essentially been supported by Monte Carlo studies.<sup>8–10</sup> The secondary structure of amylose in DMSO has also been interpreted controversially. While some authors describe it as a random coil,<sup>6,11,12</sup> others consider it to be rigidly or at least openly helical.<sup>13–15</sup> It has been pointed out that an influence of molecular weight on the global amylose structure may not be neglected in this respect.<sup>16</sup> On the basis of NMR spectroscopic results, the existence of intramolecular hydrogen bonds between OH2 and OH3 of amylose in DMSO has been assumed,<sup>17,18</sup> which as a result of a conformational analysis is supposed to be not true for aqueous solution.<sup>19</sup> Evidence from another more recent study contradicts the occurrence of intramolecular H bonding for the case of DMSO as well.<sup>15</sup> According to Cheetham and Tao,<sup>20</sup> who performed optical rotation, limiting viscosity, and <sup>13</sup>C NMR measurements in addition to butanol and iodine

complexing experiments, the amylose conformation in water/DMSO mixtures changes from a tight helix to a looser helix and finally to a random coil with the water content increasing from 0 to 66%. Along with these transitions, the number of intramolecular OH2 to OH3 hydrogen bonds is said to diminish.<sup>20</sup>

With the intention of eventually studying inclusion complexes of amylose with a variety of organic compounds on a molecular basis, we have started to look into the stability of uncomplexed amylose in water and DMSO and mixtures thereof by use of force-field-based molecular modeling and molecular dynamics techniques. We find that we can reproduce the differing behavior of helical amylose in these solvents in that we can show an increasing helical stability with an increasing percentage of DMSO in DMSO/water mixtures. In the end, however, the entropy driven intermolecular interactions win over intramolecular hydrogen bonds with the result that the helical structure transforms to a random coil conformation.

## ■ MATERIALS AND METHODS

**Generation of a V-Amylose Molecular Model.** The molecular model of V-amylose employed in this study was derived from X-ray fiber diffraction data<sup>1</sup> of thin amylose–DMSO films. Following a mathematical procedure, the provided set of atomic coordinates was amplified to yield a 6-fold left-handed amylose helix comprising 55 glucose residues.

**General Setup of Molecular Dynamics Simulations.** All calculations were carried out with the simulation program GROMACS using the GROMOS96 force field<sup>21,22</sup> together with the DMSO model proposed by Geerke et al.<sup>23</sup> and either the simple point charge (SPC) water model,<sup>24,25</sup> the SPC/E

Received: July 26, 2011

Published: July 26, 2011

**Table 1.** Overview of the Simulated Water DMSO Systems: Number of Molecules, Water Mass Fraction  $\omega$ , Water Mole Fraction  $\chi$ 

H <sub>2</sub> O	DMSO	$\omega(\text{H}_2\text{O})$	$\chi(\text{H}_2\text{O})$
29124	0	1.00	1.00
23596	1128	0.83	0.95
17759	2400	0.63	0.88
13028	3521	0.46	0.79
6870	4903	0.24	0.58
0	6869	0.00	0.00

model,<sup>26</sup> or the TIP4P model.<sup>27</sup> The parametrization of the polysaccharide model was done in accordance with the parameters described by Lins and Hünenberger.<sup>28</sup>

**Preparation of Solvent Mixtures.** In a preliminary series of simulations, starting configurations for six solvent compositions were generated (water mass fractions  $\omega_{\text{water}} = 0.0, 0.2, 0.4, 0.6, 0.8, 1.0$ ), investigating the performance of three different water models: SPC, SPC/E, and TIP4P. To this end, every mixture was simulated for 25 ns with a time step of 2 fs by means of the leapfrog integrator.<sup>29</sup> The temperature was maintained at 298.15 K and the pressure at 1.0 bar using the V-rescale<sup>30</sup> and the Berendsen algorithm,<sup>31</sup> respectively. Isothermal compressibilities for the pure solvents were set equal to the experimental values of  $8.718 \times 10^{-4}$  (kJ mol<sup>-1</sup> nm<sup>-3</sup>)<sup>-1</sup> for DMSO<sup>32</sup> and  $7.51 \times 10^{-4}$  (kJ mol<sup>-1</sup> nm<sup>-3</sup>)<sup>-1</sup> for water,<sup>33</sup> while a linear combination of these values was assigned to the water/DMSO mixtures.

The LINCS procedure<sup>34</sup> with a fourth-order expansion of the constraint coupling matrix was applied to constrain all bond lengths and all bond angles involving H atoms. Van-der-Waals interactions were treated using a twin-range cutoff scheme.<sup>35</sup> Within a spherical short-range cutoff radius of 0.8 nm, the van-der-Waals energy was calculated every time step on the basis of a neighbor list updated every five time steps. The medium-range interactions up to a long-range cutoff radius of 1.4 nm were evaluated simultaneously with each neighbor list update and kept constant between re-evaluations. To account for electrostatic interactions, the reaction-field method<sup>36</sup> was employed with a cutoff of 0.8 nm, assigning a relative dielectric permittivity of 46<sup>32</sup> and 78.5<sup>33</sup> to pure DMSO and pure water, respectively. For the mixtures, linear combinations of these values were used.

As a measure of quality for the equilibration of the different systems, the potential energy and the density  $\rho$  were monitored during the preliminary simulations, with the latter being compared to experimental data<sup>37</sup> (see Figure 3). As a result, the models SPC/E and SPC were chosen to be used in all subsequent calculations.

**Amylose MD Simulations.** The dynamic behavior of the amylose helix was simulated in water–DMSO mixtures at six different compositions (water mass fractions  $\omega_{\text{water}} = 0.0, 0.24, 0.46, 0.63, 0.83, 1.0$ ; see Table 1). For this purpose, the model was centered in a dodecahedral box with a volume of approximately 885 nm<sup>3</sup> and solvated by means of the previously prepared solvent sets. After being subjected to short energy minimization simulations (1. steepest descent algorithm: maximum step size 0.01 nm, force tolerance 10 kJ mol<sup>-1</sup> nm<sup>-1</sup>; 2. conjugated gradient algorithm: maximum step size 0.001 nm,

force tolerance 1 kJ mol<sup>-1</sup> nm<sup>-1</sup>; not more than 1000 steps either simulation), each of the systems thus generated was simulated in a series of five MD simulations for a time of 25.2 ns, employing an identical MD setup to that for the preliminary simulations (*vide supra*). This yields a total number of 55 MD simulations, with 5 × 5 simulations involving SPC/E water, 5 × 5 simulations with SPC water, and 5 simulations in pure DMSO. In addition to that, three analogous simulations were carried out over an amplified period of 100 ns, one in each of the pure solvents.

The number of hydrogen bonds was counted with the program g\_hbond in GROMACS, applying cutoffs of 3.5 Å for the distance O<sub>Donor</sub>–O<sub>Acceptor</sub> and of 30° for the angle H–O<sub>Donor</sub>–O<sub>Acceptor</sub>. Subsequently, the absolute numbers were evaluated on the basis of moving averages with subsets of 10 ps for the simulation interval between 0 and 0.05 ns, of 100 ps for 0.05 to 0.125 ns, and of 250 ps for the rest of the trajectory. In reading the calculated values, fractional numbers were rounded to the next integer; i.e., a value of 49.5 was interpreted as of 50 H bonds, for instance.

## RESULTS AND DISCUSSION

**Amylose Structure.** In preparing our conformational studies on amylose single helices in solution, the reproduction of an idealized three-dimensional V-amylose model as a basis for our work turned out to be a nontrivial problem. The use of comparable models has been scarcely reported, including the work of Immel and Lichtenhaler on the hydrophobic topography of amylose<sup>38</sup> where a V-amylose helix comprising 30 glucose residues was employed. Structural data available in the literature usually are limited to the atomic coordinates of one glucose residue and specification of the space group with the respective unit cell measures.<sup>1–4</sup> On the basis of these data, other residues can be generated by applying the 6<sub>5</sub>-helix symmetry operation, which of course may be accomplished by means of suitable crystallographic software. In the following, we describe an alternative mathematical procedure, that is readily doable with every spreadsheet program and which is easily adaptable to the generation of other amylose helices as well.

The molecular model of V-amylose employed in this study was derived from atomic coordinates based on X-ray fiber diffraction data.<sup>1</sup> Starting from the given position  $\vec{x}_i$  of an atom X<sub>i</sub> in glucose unit *i*, every analogous atom X<sub>i+1</sub> in glucose unit *i* + 1 of the amylose chain can be localized according to the recursive mathematical sequence

$$\vec{x}_{i+1} = \begin{pmatrix} \cos(-2\pi/n) & -\sin(-2\pi/n) & 0 \\ \sin(-2\pi/n) & \cos(-2\pi/n) & 0 \\ 0 & 0 & 1 \end{pmatrix} \cdot \vec{x}_i + \begin{pmatrix} 0 \\ 0 \\ p/n \end{pmatrix} \quad (1)$$

where *i* is the glucose residue number, *n* = 6 is the number of repeating units per turn, and *p* = 8.05 represents the helix pitch in Ångströms. In detail, the formula consists of a rotational matrix, generating a clockwise turn through 60° around the *z* axis, and a displacement vector that results in a translational movement by one-sixth of the helix pitch in the *z* axis direction. This amplification procedure creates the required geometry of a 6-fold left-handed helix (Figure 1). It, however, implies that adjacent monosaccharide units overlap with atoms O4 and O1. Hence, the coordinates of the redundant atoms O1, H1, and H4 were

deleted in each contemplable position, respectively, so that the generated overlapping monosaccharide units could be concatenated by glycosidic bonds.

In this manner, an amylose strand of nine 6-fold turns of overall  $S_4$  glucose residues plus one additional capping unit was generated ( $C_{330}H_{552}O_{276}$ , see Figure 2). The resulting helical structure measures about 5.4 Å in inner and 13.5 Å in outer diameter, respectively, and is about 73.8 Å long.

**Solvent Mixtures.** Six varying solvent compositions were provided for the amylose MD simulations, comprising pure water, pure DMSO, and in addition four different binary mixtures.

During the simulations for preparing the solvent starting configurations, the status of equilibration was monitored by means of the potential energy and the mass density  $\rho$  of the systems. Despite the fact that these parameters leveled off sufficiently within the first 100 ps, a total of 1 ns was provided to ensure equilibration.

In order to compare and classify the performances of the three employed water models in interaction with DMSO, the mass density  $\rho$  was evaluated over the whole simulation period of 25 ns, in this case leaving a margin of 0.2 ns for equilibration (Figure 3).

Obviously, the models generally underestimate the experimental density of the various water DMSO configurations. For pure water, the mean relative deviation is 3.3% in the case of the SPC model, while SPC/E and TIP4P obtain better approaches with 0.8% and 1.3% difference, respectively. For absolute DMSO, the simulated value averages 1.4% too low. Similar values for the DMSO model and SPC water were previously reported by Geerke et al.<sup>23</sup>

Correlation coefficients (Pearson's  $r$ ) between the calculated data sets and the experimental record are 0.985 for SPC, 0.996 for SPC/E, and 0.991 for TIP4P. Hence, the nonlinear curvature

of the experimental density graph is sufficiently well reproduced by all three of the models, with slightly better performances of SPC/E and TIP4P.

Taking into account the higher level of complexity in TIP4P and the resulting greater computational costs as compared to SPC/E and SPC, this model was ruled out for further use in this study. SPC/E, offering the best results at comparatively low computational expense, was considered to be most suitable for our purposes and was therefore employed as the main water model in all subsequent amylose MD simulations. Moreover, all simulations were also carried out with SPC water for further validation, which is closely related to SPC/E and thus does not require any additional setup procedures. For reasons of simplicity and comprehensibility, only the results obtained using the SPC/E model will be presented in the following.

**Characterization of the Amylose Helix.** The stability of a V-amylose helical structure essentially relies on intramolecular hydrogen bonds,<sup>20</sup> distinguishable into two types of hydrogen bonds that we define as interturn H bonds ( $O_6-O_2$  and  $O_6-O_3$ ) and intraturn H bonds between adjacent glucose units ( $O_2-O_3$ ), respectively (Figure 4). The hydrogen bond  $O_6-O_3$  is taken into account despite its rather weak nature in the crystal structure,<sup>39</sup> as the actual O–O distances within the amylose molecule are expected to fluctuate considerably in solution. Another noteworthy issue with respect to the intramolecular H-bond pattern is the effect of hydrogen bond cooperativity. As hydroxyl groups can build both accepting and donating hydrogen bonds, a continuous network can be established. The resulting mutual polarization in the functional groups leads to an enhanced stability of their hydrogen bonding network.

The idealized amylose model used in this study exhibits a total number of intramolecular hydrogen bonds  $N_{\text{tot}}$  of 152, which will be used as a reference point in the characterization of the helical content of the employed amylose (Figure 4).

**Degradation of the Helical Secondary Structure.** In all of the 55 amylose simulations, a continuous degradation of the helical structure can be observed. After a simulated time of 25 ns, the amylose chain independently of the solvent configuration has adopted an apparently randomly coiled conformation, and no helical content is evident anymore. This trend can numerically be tracked on the basis of the sum of intramolecular hydrogen bonds  $N_{\text{tot}}$ , which roughly speaking shows a continuous decline over the simulation time. This is true in water, as well as in DMSO and in mixtures thereof and finally results in a rather low number of intramolecular hydrogen bonds after 25 ns in each case (Figure 5).

**Solvent Composition Impact on the Rate of Decomposition of the Helical Secondary Structure.** A comparison of the amylose structures in DMSO and water with respect to their

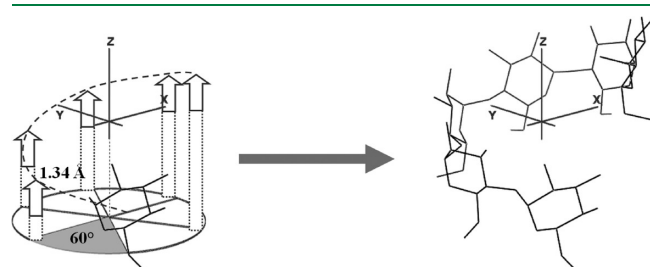


**Figure 1.** Schematic representation of the V-amylose modeling. By successive application of eq 1 to the atomic coordinates of one given glucose residue, a helical conformation is generated. The symmetry operation consists of a clockwise turn through  $60^\circ$  around the  $z$  axis and a displacement by 1.34 Å in the  $z$  axis direction.

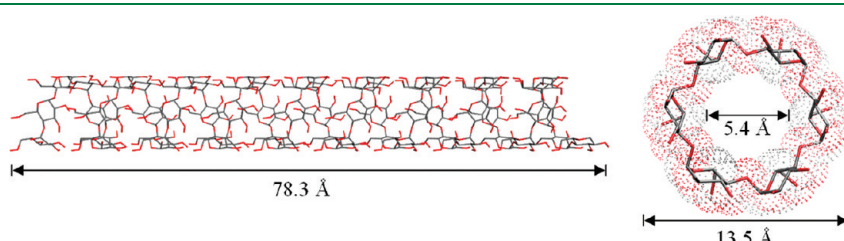


**Figure 2.** Views of the calculated amylose model. Lateral view and view along the helix axis ( $z$  axis) with an estimated molecular surface.

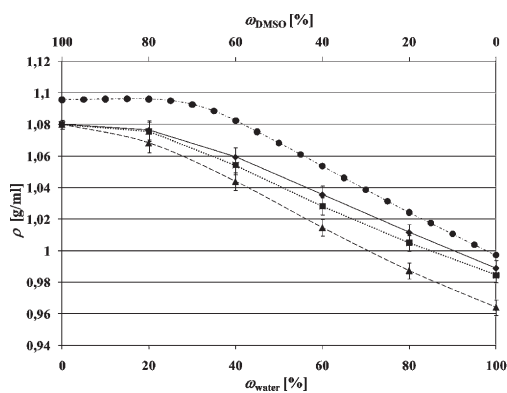


**Figure 3.** Density values from MD simulations and experimental data<sup>37</sup> versus mass fractions  $\omega$  of water/DMSO in the solvent mixtures. The points were calculated as mean values of the trajectory (25 ns) of a given MD simulation, omitting an initial equilibration period of 0.2 ns. The error bars represent  $2\sigma$  confidence intervals, with  $\sigma$  being the estimated standard deviation.

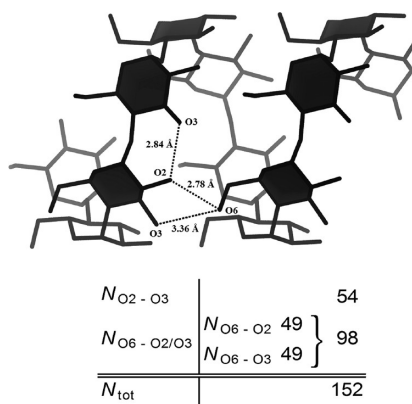
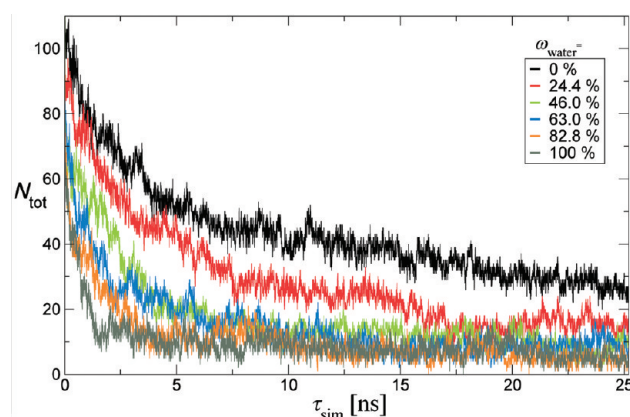


**Figure 4.** Schematic representation of the particular intramolecular hydrogen bonds in V-amylose and their respective length values. The table provides the absolute counts of the H bonds occurring in the used model structure (55 glucose residues).

time-dependent development, however, reveals significant differences. An illustration for this is shown in Figure 6, which depicts schematic snapshots of the amylose molecule at selected points in simulation time. In general, the total number of hydrogen bonds present in the amylose helix after its generation is already reduced to 80 in water and to 99 in DMSO, respectively, after initial equilibration with the steepest descent and conjugated gradient algorithms. In the following MD simulation using water,  $N_{tot}$  is reduced rather quickly after only 0.21 ns from 80 to 50 ( $\equiv N_{tot}/N_{max} \approx 30\%$ ), resulting in a visible distortion of the helical structure, while in DMSO at the same time only a minor loss of H bonds and only slight deviations from the ideal helix can be recognized. It takes about 4.71 ns until the number of intramolecular H bonds in DMSO has reached a similar value ( $N_{tot} = 47$ ). By this time, the structure in water already appears to be randomly orientated. Even after 25 ns, when the amylose model does not exhibit any obvious helix content anymore in either water or DMSO, there is still an unambiguously higher  $N_{tot}$  in the aprotic solvent DMSO as compared to water (17 versus 5). In this respect, it is noteworthy



$\omega_{water}$ [%]	$N_{tot}$ (25 ns)
0.0	21.70
24.4	14.74
46.0	10.44
63.0	7.48
82.8	9.90
100.0	7.72

**Figure 5.** Reduction of  $N_{tot}$  over time in one exemplary series of MD simulations in SPC/E water. The table provides values for  $N_{tot}$  after 25 ns averaged over all five simulations for each solvent mixture.

that the exemplary performed MD simulations of the systems in DMSO and water over a period of 100 ns show that even beyond 25 ns the numbers of H bonds continue to decrease, eventually leveling out near zero (Figure 7). A differentiation of amylose structures on the basis of intramolecular hydrogen bonds is then not possible anymore.

In the case of water, the substitution of intramolecular by intermolecular hydrogen bonds results in a considerable gain of Coulomb interactions for the amylose molecule (Figure 8). A comparison of the energy balances at the beginning ( $\approx -11\ 700$  kJ/mol) and at the end ( $\approx -16\ 600$  kJ/mol) of the 100 ns simulation time yields a benefit of around 4900 kJ/mol. In contrast, the unwinding of the helix in DMSO is obviously not energetically favorable in this context (deficit of 1300 kJ/mol), so there must be a considerable influence of entropic factors acting as a driving force for the decay process.

Considering the entire series of six different solvent compositions, one can detect a distinct gradual tendency in the rate of the helical decay. Essentially, the number of H bonds ( $N_{tot}$ ) diminishes most rapidly in pure water and more slowly when the DMSO mass fraction  $\omega_{DMSO}$  is increased. This is shown in Figure 9. Starting from pure DMSO, the simulation time  $\tau_{sim}$  at which  $N_{tot}$  falls below values of 50%, 40%, and 30% of the original value  $N_{max}$  of 152 decreases with an increasing percentage of water. The shape of the three curves is very similar and indicates a gradual tendency of the decomposition

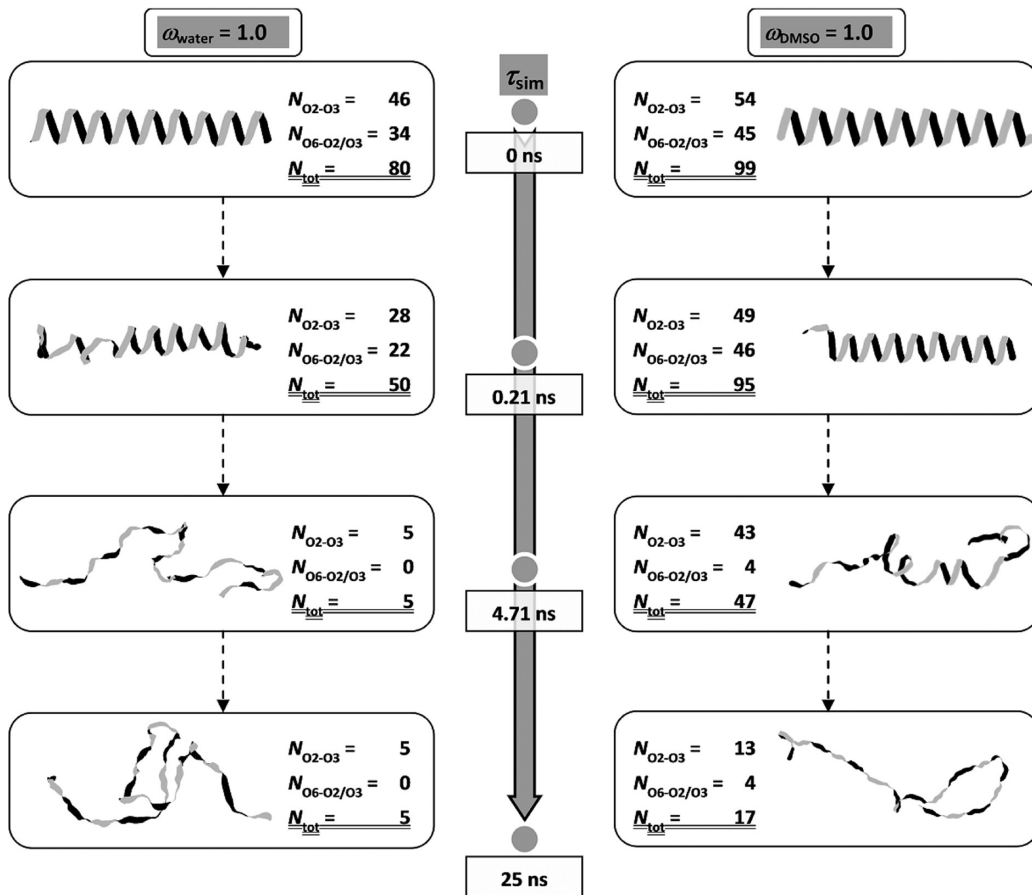


**Figure 6.** Corresponding snapshots of the amylose secondary structure (schematic) from two exemplary MD simulations in pure water (left) and pure DMSO (right). The depicted conformations were chosen at a point in simulation time where the ratio  $N_{\text{tot}}/N_{\text{max}}$  in the two solvents is 0.3, which is after 0.21 ns in water, while only after 4.71 ns in DMSO. In addition, the starting point is shown, i.e., after geometrical optimization using steepest descent and conjugated gradient energy minimization, as well as the end point of the simulation after 25 ns.

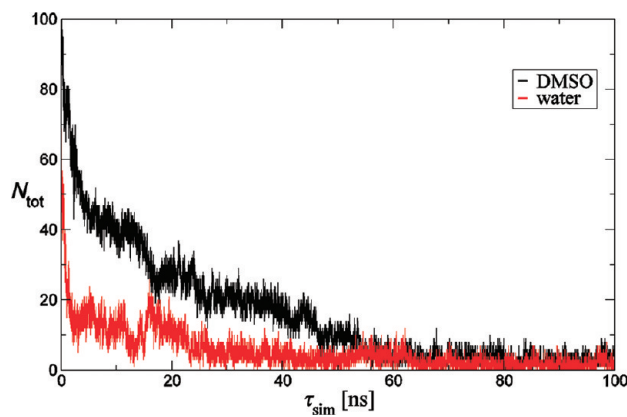


**Figure 7.** Development of  $N_{\text{tot}}$  over 100 ns in pure DMSO and pure water.

rate of the helical secondary structure depending on the solvent composition. Noteworthy is the change of the slope at  $\omega_{\text{water}} \approx 63\%$ , which resembles the discontinuities in a number of physical properties of amylose reported in the literature.<sup>20,6</sup> In addition, the results compare well to the experimental finding that an amylose helix is more stable in 80% to 100% DMSO than in water.<sup>40,20</sup>

This behavior can be explained by comparing the interaction of the two solvents, water and DMSO, with the amylose helix (Figures 10 and 11). The water molecule is strongly dipolar and is capable of forming a maximum of four hydrogen bonds at a time, two as a hydrogen donor and two as a hydrogen acceptor. Furthermore, it is small enough to deeply intrude into the polysaccharide's secondary structure, thereby weakening the intramolecular hydrogen bond network. DMSO, on the other hand, is equally polar but can only act as a 2-fold hydrogen bond acceptor. In addition, occupying a van der Waals volume about 4.5 times as high as that of water, and featuring a rather branched structure, DMSO is by far the bulkier molecule. Due to this sterical hindrance, it is impossible for DMSO to bind to each of the hydroxyl groups on the amylose surface (Figure 11). Nevertheless, it is conceivable that one DMSO molecule for instance simultaneously binds both OH<sub>2</sub> and OH<sub>3</sub> of one single or two adjacent glucose molecules. However, such an intensive interaction would create a rather unfavorable situation as it would lower the partial negative charge of the DMSO oxygen and thus would result in two rather weak H bonds. Instead, a more convenient situation would exist, if one DMSO molecule each attached to only one or two of the three different hydroxyl groups in the amylose chain, since this would leave two or at least one OH group per glucose residue free, which in turn would then be available for intramolecular hydrogen bonding. This results in a

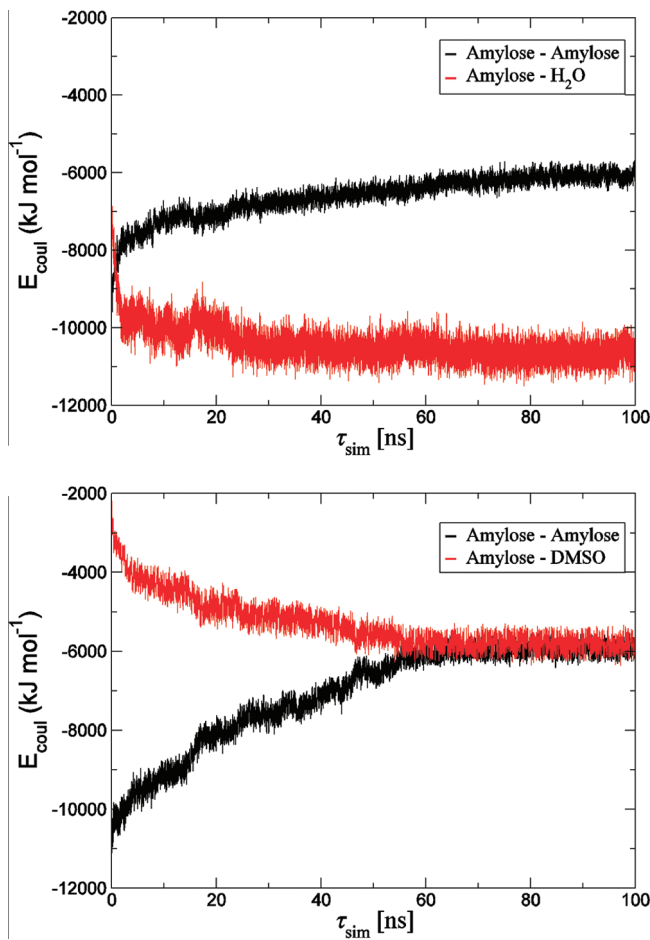


**Figure 8.** Intra- and intermolecular Coulomb interaction energies of amylose over 100 ns in pure DMSO and pure water.

strengthening effect of cooperative hydrogen bonding described in the literature.<sup>40</sup>

As a result, after equilibration of the water box including the OH groups of amylose with an otherwise constrained helical structure, we find water molecules within H bond distance to every hydroxyl group of amylose. In a representative snapshot of this simulation, shown in Figure 10, one can see that at a given time adjacent OH<sub>2</sub> and OH<sub>3</sub> groups can simultaneously be hydrated by water molecules, independent of being situated on adjacent glucose residues (A) or on the same residue (B). The spatial demand of water is small enough that the OH<sub>6</sub> groups close by are at the same time also hydrated and are in some cases even coordinated by two water molecules (C).

In contrast, as DMSO molecules are about 4.5 times as voluminous as water molecules and can only act as a 2-fold direction-dependent hydrogen bond acceptor, DMSO only incompletely binds the amylose hydroxyl groups, and there are always one or two OH groups free per glucose unit. As a result, we find a lower molar density of DMSO on the helix surface as compared to that of water (Figure 11).

Interestingly, the graph in Figure 9 shows a strongly nonlinear behavior for the disruption of the helical structure, featuring a very flat slope in the region of  $\omega_{\text{water}} \gtrsim 60\%$  and a rapid increase when more DMSO is added to the mixture, indicating that there is a limiting concentration of DMSO above which the decay of intramolecular hydrogen bonds in amylose is progressively

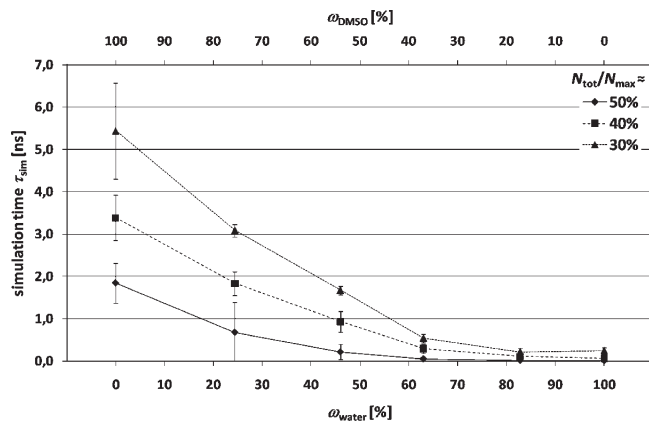


**Figure 9.** Average simulation period for a reduction of  $N_{\text{tot}}/N_{\text{max}}$  below values of about 50%, 40%, and 30% of the initial value as a function of solvent composition. For example, the upper line gives the results for the six solvent mixtures used from pure DMSO (left) to pure water (right) and indicates the average point in simulation time at which the total number of intramolecular H bonds of amylose  $N_{\text{tot}}$  in the given solvent mixture has decreased to 30% of its initial value ( $N_{\text{max}} = 152$ ).

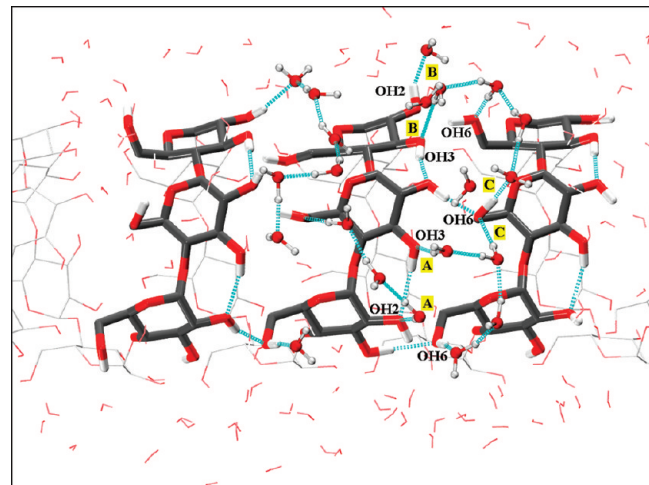


**Figure 10.** Orthographic snapshot of a V-amylose molecule solvated by water. Dashed lines (cyan) indicate hydrogen bonds. For the sake of clarity, only selected water molecules are drawn in CPK style. Due to their small size and ability to donate and accept hydrogen bonds in four different directions, water molecules can bind theoretically every hydroxyl group of amylose at one time. The picture shows examples for simultaneous hydration of OH<sub>2</sub> and OH<sub>3</sub> on adjacent glucose residues (A) as well as on the same residue (B). The respective opposing OH<sub>6</sub> groups are also in a hydrated state, in one case even coordinated by two water molecules (C).

decelerated. Qualitatively similar discontinuities have been observed for a number of physical properties of amylose in the regarded binary system, such as limiting viscosity<sup>20</sup> and specific optical rotation.<sup>6</sup> Moreover, evidence has been presented that a minimum volume fraction of  $\sim 60\%$  water (equivalent to  $\omega_{\text{water}} \approx 0.6$ ) is necessary for amylose to be capable of forming detectable complexes with butanol<sup>20</sup> or iodine.<sup>18,20</sup> These observations have partially been attributed to the relative effectiveness of water and DMSO in solvating amylose, i.e., a competitive behavior of the two solvents.<sup>18,20</sup> Accordingly, the role of water in the

solvation of amylose and its influence on the helical structure can be considered to be predominant over that of DMSO exclusively in the region of  $\omega_{\text{water}} \gtrsim 60\%$ , which is equivalent to a molar ratio of water/DMSO of at least 6:1 and essentially coincides with the flat region of the curves in Figure 9.

At higher DMSO concentrations, there is presumably not enough free water present for an effective amylose hydration due to the formation of DMSO hydrates. Data on excess heat of mixing, density, and viscosity<sup>41</sup> as well as NMR<sup>42</sup> and neutron diffraction experiments<sup>43,44</sup> and molecular dynamics simula-

tions<sup>43,45–47</sup> have revealed that these water–DMSO complexes consist of two or three water molecules attached to one single DMSO molecule strongly stabilized by hydrogen bonds. The higher basicity of the DMSO oxygen in comparison with the water oxygen makes it a better acceptor for available hydrogen bonds, consequently making the DMSO hydrates more energetically favorable than just water–water interactions. The reduced number of mobile water molecules in the mixture results in decreased stress on the intramolecular hydrogen bonding network of amylose. It is even conceivable that DMSO hydrates interact with amylose hydroxyl groups in a similar way as DMSO molecules do, thereby strengthening the remaining amylose H bonds.<sup>40</sup> Hence, the predefined helical conformation is degraded at a lesser rate than in pure water.

Above the threshold of  $\omega_{\text{DMSO}} \approx 80\%$ , which corresponds to a molar ratio of DMSO/water of about 1:1, solvation of amylose by free DMSO may be expected to predominate over solvation by water and hydrated DMSO, respectively, particularly since DMSO is the stronger hydrogen bond acceptor than water.<sup>40</sup> This leaves a large percentage of the amylose H-bonding network intact, which yields a further increase in conformational stability accompanied by another rise in the slope of the time graphs in Figure 9.

**Differentiation of Hydrogen Bonds.** The differentiation of the intramolecular hydrogen bonds was made in terms of interturn and intraturn character, referring to turns as the repetitive loops of the helical structure. O<sub>2</sub>–O<sub>3</sub> and O<sub>6</sub>–O<sub>2/3</sub> H bonds were treated as equivalent since either of them represents an interturn connection within the same pair of glucose residues (Figure 4).

Figure 6 reveals that O<sub>2</sub>–O<sub>3</sub> and O<sub>6</sub>–O<sub>2/3</sub> H bonds are degraded at unequal rates, in water as well as in DMSO. At the starting point (0 ns), i.e., after energy minimization, more than half of the O<sub>6</sub>–O<sub>2/3</sub> H bonds have already been destroyed, probably in part due to the fact that one of the two bonds had to be considered weak even in the underlying crystal structure.

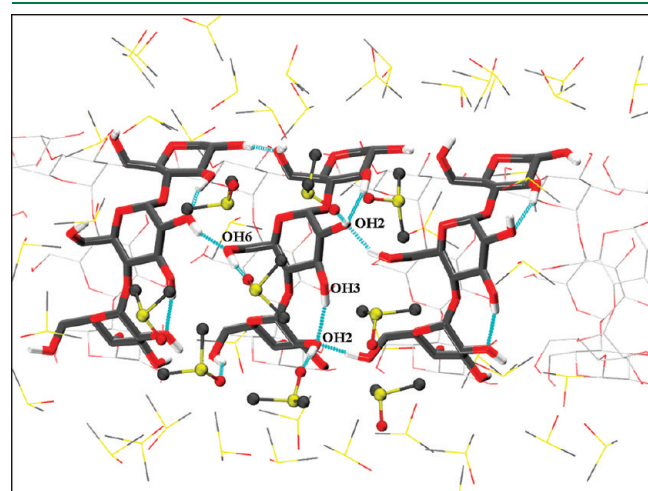


**Figure 11.** Orthographic snapshot of a V-amylose molecule solvated by DMSO. Dashed lines (cyan) indicate hydrogen bonds. For the sake of clarity, only selected DMSO molecules are drawn in CPK style. Note the lower molar density of DMSO on the helix surface as compared to that of water (Figure 10).

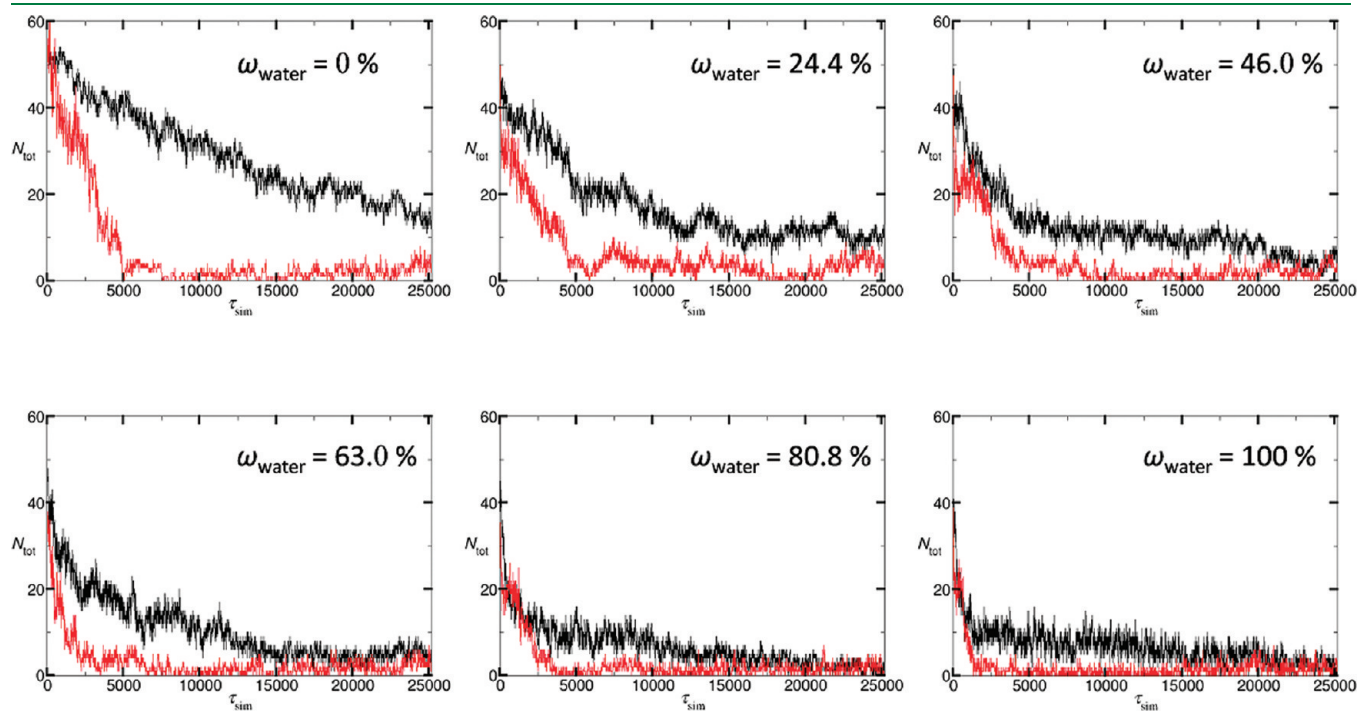


**Figure 12.** Total number of H bonds  $N_{\text{O}_2-\text{O}_3}$  (black) and  $N_{\text{O}_6-\text{O}_2/3}$  (red) versus simulation time (ps). Each of the six solvent ratios investigated is shown as a representative graph from the series of five MD simulations.

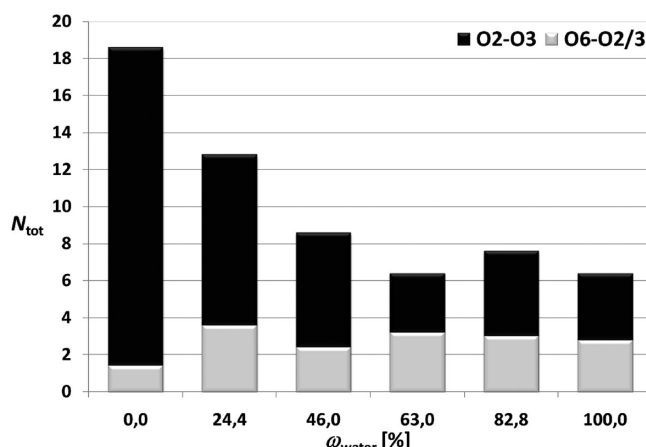


**Figure 13.** Average numbers of inter- and intraturn H bonds vs  $\omega_{\text{water}}$ , obtained after a simulation time of 25 ns.

In the following simulation period, there is a permanent dominance of intraturn over interturn H bonds. In water, this remains on the same order of magnitude, while in DMSO, it distinctly increases between 0.21 and 4.71 ns. From that point on to the end of the simulation, the difference diminishes in DMSO as the remaining number of  $O_6-O_2/3$  H bonds is close to zero anyway.

The time dependence of inter- and intraturn H bonds is given in Figure 12. While each solvent system was simulated in a series of five MD simulations, the graphs show the data of only one representative exemplary simulation. Generally, the impression of a dominance of  $O_2-O_3$  over  $O_6-O_2/3$  H bonds is confirmed here, which implies that the intraturn H bonds are retained longer than the interturn ones. From this, it can be hypothesized that the first step of the helix degradation consists of a widening of the helical pitch by breaking the interturn H bonds directed along the  $z$  axis, meaning that the helix loses its compactness in this direction.

The degree of helical curvature depends on the orientation of subsequent glucose residues toward each other, i.e., basically on the glycosidic angles  $\phi$  and  $\psi$ . Alterations of these angles directly influence the length and thus the stability of the  $O_2-O_3$  H bond but do not implicitly break it within a certain margin. The overall conformational changes that result from the sum of many of these small torsional alterations across the amylose chain are of course much more significant. As the  $O_6-O_2/3$  H bonds are situated between different turns of the helix and are therefore much more conformation dependent than the relatively fixed  $O_2-O_3$  H bonds, one can expect a greater distortion for these. This explains the longer conservation of intraturn H bonds as compared to interturn ones.

The dominance of  $O_2-O_3$  over  $O_6-O_2/3$  H bonds as seen in Figures 6 and 13 and its chronological development is by far most significant for pure DMSO and is gradually reduced along with the increasing percentage of water. As the helical loops start to come apart, the sterically demanding DMSO molecules can first of all solvate the OH6 group, having a rather exposed location remote from the glucose ring. OH2 and OH3, in contrast, cannot be solvated simultaneously, at least not until the amylose chain becomes further unfolded and is completely surrounded by the solvent. In the process of helix degradation, this leads to an increased tendency of DMSO for breaking interturn H bonds. The smaller water molecules (free or in DMSO hydrates) on the other hand can readily solvate OH2 and

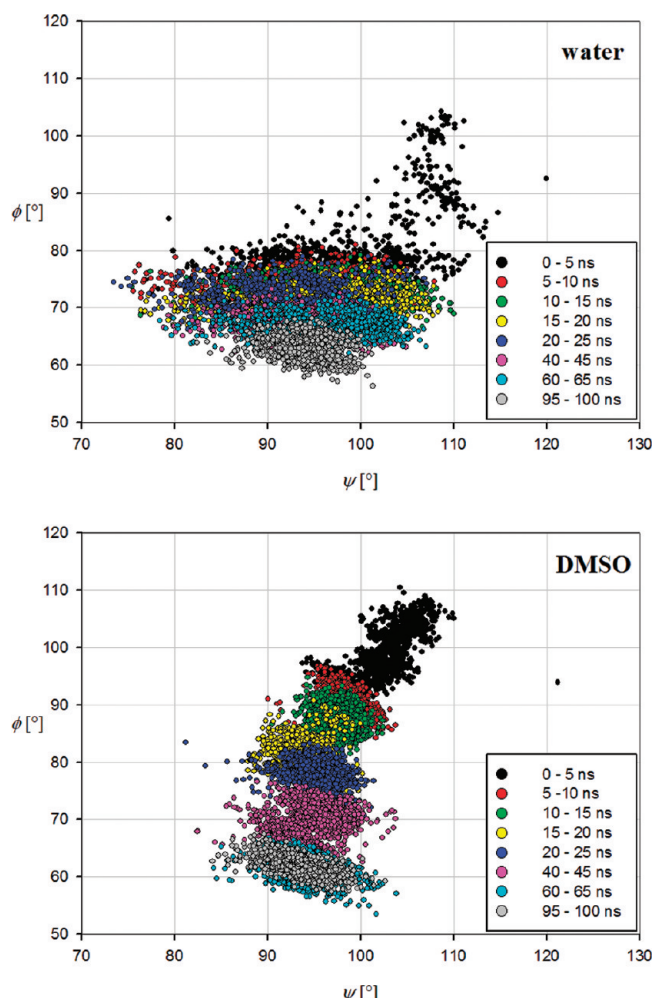


**Figure 14.** Time-dependent development of the glycosidic torsion angles  $\phi$  ( $O_5-C_1-O_4-C_4$ ) and  $\psi$  ( $C_1-O_4-C_4-C_3$ ) in 100 ns simulations using water and DMSO as solvents, respectively. Data points are shown in differently colored time intervals of 5 ns. For the sake of clarity, only selected time intervals are shown in the region between 25 and 100 ns.

OH3 at the same time so that the preference for solvation of OH6 is not as pronounced as in pure DMSO.

Furthermore, this effect can also clearly be seen at the end of the simulation. Figure 13 shows that after a simulation period of 25 ns the average  $N_{O_6-O_2/3}$  of each of the six solvent mixtures is not higher than 3.6. With regard to the standard deviation ranging from 1.1 for  $\omega_{\text{water}} = 63\%$  to 2.8 for  $\omega_{\text{water}} = 100\%$ , the difference of interturn H bonds between the solvent systems is statistically identical. There is, however, the expected trend in the respective  $N_{O_2-O_3}$  values. While there is a comparatively high average value of 17.2 for  $\omega_{\text{water}} = 0\%$ , it gradually decreases to values between 3 and 5 for  $\omega_{\text{water}} = 63\%$  to 100%. This curve shape obviously corresponds to the graphs in Figure 9 and may similarly be interpreted taking into account the specific hydrogen bonding capacities, steric features, and mixture characteristics of the two solvents, water and DMSO.

A general aspect of the parameter  $N_{\text{tot}}$  and its use in describing the helix character of amylose becomes apparent in the differentiation of hydrogen bonds as shown in Figures 6, 12, and 13. The exemplary amylose structures at 0.21 and 4.71 ns in water

and DMSO, respectively, are rated as very similar in terms of  $N_{\text{tot}}$  despite being conformationally rather different. A numerical difference only becomes visible on inspection of  $N_{\text{O}_2-\text{O}_3}$  and  $N_{\text{O}_6-\text{O}_2/3}$ . While in water, the numbers are on the same order of magnitude,  $N_{\text{tot}}$  in DMSO is almost exclusively based on O2–O3 H bonds. This finding demonstrates that the total number of intramolecular hydrogen bonds  $N_{\text{tot}}$  only to some extent correctly describes a generally defined “helical content” in the conformation of amylose. An exhaustive comparison of two such conformations in terms of their helix character, therefore, requires a weighting of the particular interturn and intraturn summands of  $N_{\text{tot}}$ .

This can alternatively be analyzed by evaluating the glycosidic torsion angle distribution, which is depicted in Figure 14 for the two 100 ns simulations in pure water and pure DMSO. In either case, the helical degradation is characterized by distinct changes of the dihedral angles  $\phi$  (O5–C1–O4–C4) and  $\psi$  (C1–O4–C4–C3). Especially  $\phi$  undergoes a pronounced decrease, namely, from an average  $107^\circ$  ( $\tau_{\text{sim}} = 0$  to 0.1 ns) to an average  $62^\circ$  (95 to 100 ns) in DMSO and from  $102^\circ$  to  $63^\circ$  in water. The major part of this development proceeds during the first 5 ns of the simulation in water, whereas the process is more extended in DMSO, which parallels the pathways of the respective number of intramolecular H bonds  $N_{\text{tot}}$  (Figure 7).

## ■ CONCLUSION

**Modeling of Amylose Structures.** In spite of the extensive research on structural features of V-amylose, the availability of atomic coordinates for this system is rather limited. X-ray and electron diffraction data in the literature<sup>1–4</sup> yield structural data of one glucose unit and do not provide atomic data for an amplified structure of monomers in either one of the known amylose conformations. Building an idealized model structure of customized length, as the one used in this study, therefore requires the utilization of adequate crystallographic software that allows performing the respective symmetry operations in order to generate a molecule coordinate file. As an alternative, the rather simple linear algebraic approach presented in this work has the advantage that it can technically be managed by a common spreadsheet program or even a programmable calculator.

**Modeling of Water/DMSO Mixtures.** In preparation for our studies on the behavior of an amylose helix in water, DMSO, and various mixtures thereof, we have compared the performances of three water models (SPC,<sup>24,25</sup> SPC/E,<sup>26</sup> and TIP4P<sup>27</sup>) in terms of their ability to reproduce an experimental density record<sup>37</sup> of various water DMSO mixtures by molecular dynamics procedures (Figure 3). All three models reproduce the known nonlinear density behavior of the considered series of binary solvent mixtures to a satisfactory degree. Despite its lower level of complexity as compared to TIP4P, the SPC/E model provides the best approximation to the experimental density curve. It can thus be recommended for being used in simulations of water DMSO mixtures employing the DMSO model by Geerke et al.<sup>23</sup>

**Amylose MD Simulations.** Our results suggest that with enough time given for interaction between amylose and the solvent the helix is not stable in either water or DMSO and rather unfolds to a randomly coiled structure. The intramolecular H bonds between OH2 and OH3, OH6 and OH2, and OH6 and OH3 hydroxyl groups of adjacent glucose residues, which are responsible for maintaining the helical structure, are lost in favor of intermolecular H bonds between the solvent and the OH

groups of amylose combined with a gain in entropy. We can reproduce the experimentally known difference in helix stability<sup>20,40</sup> with a progressively faster disruption of the helical structure with an increasing percentage of water in water/DMSO mixtures, as shown in Figures 6 and 9. While Figure 6 gives a good visual impression of the different behavior of the amylose helix in water and DMSO, respectively, the strongly nonlinear behavior of the graph in Figure 9 even reflects the observed discontinuities in physical properties of the system described in the literature, such as limiting viscosity,<sup>20</sup> specific optical rotation,<sup>6</sup> and the ability to form detectable complexes with butanol<sup>20</sup> or iodine.<sup>18,20</sup> Obviously, water molecules promote the helix decay due to their small size and increased hydrogen bonding capabilities as compared with DMSO molecules. Between approximately 40% and 80% DMSO, the formation of DMSO hydrates decelerates the helix degradation by reducing the number of free water molecules, and above 80% DMSO, the excess of DMSO molecules leads to another even more distinct deceleration of the process.

Our modeling results furthermore can differentiate between the types of H bonds involved in stabilizing the helical amylose structure. We can show that there is a dominance of O2–O3 versus O6–O2/3 H bonds of adjacent glucose residues; i.e., the intraturn H bonds are more stable than the interturn ones (Figures 6, 13). This result suggests that helix degradation begins with a widening of the helical pitch by breaking the interturn H bonds directed along the z axis, accompanied by a loss of compactness in this direction. On account of the higher steric demand of DMSO molecules relative to water molecules, their preference for breaking O6–O2/3 H bonds is considerably more significant, especially as the OH6 groups are more readily accessible than the OH2 and OH3 groups close to the glucose ring.

In summary, our simulations show that, independent of the solvent, the helical structure is destroyed in water as well as in DMSO, with the distinct difference of a slower interference of DMSO with the structure preserving intramolecular H bonds of amylose. In the long run, however, the vast excess of solvent molecules substitutes the intra- with intermolecular H bonds, which is driven by entropic factors.

A stable V-helical amylose structure, therefore, requires more stabilization than can be derived from intermolecular H bonds. The most commonly known example is of course the well-known complex of iodine and starch.<sup>48,49</sup>

Stabilization in this case is gained from the inside of the helix as amylose and iodine form an inclusion complex. Such complexes are also known with organic compounds, even as small as butanol.<sup>50</sup> More prominent examples, however, are inclusion complexes from amylose and fatty acids or fatty alcohols<sup>51</sup> and those formed by vine-twining polymerization, when glucose is enzymatically polymerized around synthetic polymers.<sup>52,53</sup> These systems are of great potential industrial use, and simulations along these lines are, therefore, in progress in our laboratory.

## ■ AUTHOR INFORMATION

### Corresponding Author

\*E-mail: fels@uni-paderborn.de.

## ■ REFERENCES

- (1) Rappenecker, G.; Zugenmaier, P. *Carbohydr. Res.* **1981**, *89*, 11–19.
- (2) Winter, W. T.; Sarko, A. *Biopolymers* **1974**, *13*, 1461–1482.

- (3) Murphy, V. G. *Biopolymers* **1975**, *14*, 1487–1501.
- (4) Brisson, J.; Chanzy, H.; Winter, W. T. *Int. J. Biol. Macromol.* **1991**, *13*, 31–39.
- (5) Brant, D. A.; Dimpfl, D. L. *Macromolecules* **1970**, *3* (5), 655–664.
- (6) Dintzis, F. R.; Tobin, R. *Biopolymers* **1969**, *7*, 581–593.
- (7) Elmgren, H. *Biopolymers* **1984**, *23*, 2525–2541.
- (8) Jordan, R. C.; Brant, D. A.; Cesàro, A. *Biopolymers* **1978**, *17*, 2617–2632.
- (9) Gagnaire, D.; Pérez, S.; Tran, V. *Carbohydr. Polym.* **1982**, *2*, 171–191.
- (10) Kitamura, S.; Okamoto, T.; Nakata, Y.; Hayashi, T.; Kuge, T. *Biopolymers* **1987**, *26*, 537–548.
- (11) Everett, W. W.; Foster, J. F. *J. Am. Chem. Soc.* **1959**, *81*, 3464–3469.
- (12) Banks, W.; Greenwood, C. T. *Carbohydr. Res.* **1968**, *7* (4), 414–420.
- (13) Cowie, J. M. G. *Makromol. Chem.* **1961**, *42*, 230–247.
- (14) Fujii, M.; Honda, K. *Biopolymers* **1973**, *12*, 1177–1195.
- (15) Sugiyama, H.; Nitta, T.; Horii, M.; Motohashi, K.; Sakai, J.; Usui, T.; Hisamichi, K.; Ishiyama, J. *Carbohydr. Res.* **2000**, *325*, 177–182.
- (16) Nakanishi, Y.; Norisuye, T.; Teramoto, A. *Macromolecules* **1993**, *26*, 4220–4225.
- (17) St-Jacques, M.; Sundararajan, P. R.; Taylor, K. J.; Marchessault, R. H. *J. Am. Chem. Soc.* **1976**, *98*, 4386–4391.
- (18) Peng, Q.-J.; Perlin, A. S. *Carbohydr. Res.* **1987**, *160*, 57–72.
- (19) Perez, S.; Vergelati, C. *Polym. Bull.* **1987**, *17*, 141–148.
- (20) Cheetham, N. W. H.; Tao, L. *Carbohydr. Polym.* **1998**, *35*, 287–295.
- (21) Van Der Spoel, D.; Lindahl, E.; Hess, B.; Groenhof, G.; Mark, A. E.; Berendsen, H. J. J. *Comput. Chem.* **2005**, *26*, 1701–1718.
- (22) van Gunsteren, W. F.; Billeter, S. R.; Eising, A. A.; Hünenberger, P. H.; Krüger, P.; Mark, A. E.; Scott, W. R.; Tironi, I. G. *vdf Hochschulverlag*; ETH: Zürich, Switzerland, 1996.
- (23) Geerke, D. P.; Oostenbrink, C.; Vegt, N. F.; Gunsteren, W. F. *J. Phys. Chem. B.* **2004**, *108*, 1436–1445.
- (24) Berendsen, H. J.; Postma, J. P.; van Gunsteren, W. F.; Hermans, J. *Intermolecular Forces*; Pullman, B., Ed.; Reidel: Dordrecht, Holland, 1981; pp 331–342.
- (25) Ferguson, D. M. *J. Comput. Chem.* **1995**, *16*, 501–511.
- (26) Berendsen, H. J. C.; Grigera, J. R.; Straatsma, T. P. *J. Phys. Chem.* **1987**, *91*, 6269–6271.
- (27) Jorgensen, W. L.; Chandrasekhar, J.; Madura, J. D.; Impey, R. W.; Klein, M. L. *J. Chem. Phys.* **1983**, *79*, 926–935.
- (28) Lins, R. D.; Hünenberger, P. H. *J. Comput. Chem.* **2005**, *26*, 1400–1412.
- (29) Van Gunsteren, W. F.; Berendsen, H. J. *Mol. Simul.* **1988**, *1*, 173–185.
- (30) Bussi, G.; Donadio, D.; Parrinello, M. *J. Chem. Phys.* **2007**, *126*, 14101–14108.
- (31) Berendsen, H. J.; Postma, J. P.; van Gunsteren, W. F.; DiNola, A.; Haak, J. R. *J. Chem. Phys.* **1984**, *81*, 3684–3690.
- (32) Riddick, J. A.; Bunger, W. B.; Sakand, T. K. *Organic Solvents: Physical Properties and Methods of Purification*; John Wiley and Sons: New York, 1986.
- (33) Kell, G. S. *J. J. Chem. Eng. Data* **1967**, *12*, 66–69.
- (34) Hess, B.; Bekker, H.; Berendsen, H. J.; Fraaije, J. G. *J. Comput. Chem.* **1997**, *18*, 1463–1472.
- (35) van Gunsteren, W. F.; Berendsen, H. J. *Angew. Chem., Int. Ed.* **1990**, *29*, 992–1023.
- (36) Tironi, I. G.; Sperb, R.; Smith, P. E.; van Gunsteren, W. F. *J. Chem. Phys.* **1995**, *102*, 5451–5459.
- (37) LeBel, R. G.; Goring, D. A. *J. Chem. Eng. Data* **1962**, *7*, 100–101.
- (38) Immel, S.; Lichtenthaler, F. W. *Starch/Stärke* **2000**, *52*, 1–8.
- (39) Jeffrey, G. A. *An Introduction to Hydrogen Bonding*; Oxford University Press: New York, 1997.
- (40) Erlander, S. R.; Tobin, R. *Makromol. Chem.* **1968**, *111*, 194–211.
- (41) Cowie, J. M. G. *Can. J. Chem.* **1961**, *39*, 2240–2243.
- (42) Glasel, J. A. *J. Am. Chem. Soc.* **1970**, *92*, 372–375.
- (43) Soper, A. K.; Luzar, A. *J. Phys. Chem.* **1996**, *100*, 1357–1367.
- (44) Soper, A. K.; Luzar, A. *J. Chem. Phys.* **1992**, *97*, 1320–1331.
- (45) Luzar, A.; Chandler, D. *J. Chem. Phys.* **1993**, *98*, 8160–8173.
- (46) Vaisman, I. I.; Berkowitz, M. L. *J. Am. Chem. Soc.* **1992**, *114*, 7889–7896.
- (47) Borin, I. A.; Skaf, M. S. *J. Chem. Phys.* **1999**, *110*, 6412–6420.
- (48) Saenger, W. *Naturwissenschaften* **1984**, *71* (1), 31–36.
- (49) Moulik, S. P.; Gupta, S. *J. Sci. Ind. Res.* **1986**, *45*, 173–178.
- (50) Schoch, T. *J. Adv. Carbohydr. Chem.* **1945**, *1*, 247–277.
- (51) Nimz, O.; Gessler, K.; Uson, I.; Sheldrick, G. M.; Saenger, W. *Carbohydr. Res.* **2004**, *339*, 1427–1437.
- (52) Kaneko, Y.; Saito, Y.; Nakaya, A.; Kadokawa, J.-I.; Tagaya, H. *Macromolecules* **2008**, *41*, 5665–5670.
- (53) Kaneko, Y.; Beppu, K.; Kadokawa, J.-I. *Biomacromolecules* **2007**, *8* (10), 2983–2985.